Experimental and Computational Study of Multiphase Gas/ Particle Flow in a CFB Riser

Vidar Mathiesen and Tron Solberg
Telemark College (HiT-TF) and Telemark R&D Centre (Tel-Tek), N-3914 Porsgrunn, Norway

Hamid Arastoopour
Dept. of Chemical and Environmental Engineering, Illinois Institute of Technology, Chicago, IL 60616

Bjørn H. Hjertager
Aalborg University Esbjerg, DK-6700 Esbjerg, Denmark

The flow behavior in the riser of a circulating fluidized-bed reactor was studied experimentally and computationally. Laser Doppler anemometry was applied to measure the flow behavior of FCC catalysts. Particle diameter and mean and fluctuating velocity for different particle sizes were measured at different flow conditions. A typical core-annulus flow with a relative velocity between particles of different sizes was obtained. A significant radial segregation of the mean diameter was measured in the riser. A multifluid computational fluid dynamics model was developed and verified against the experimental results. The flow model is based on a Eulerian description of the phases where the kinetic theory for granular flow forms the basis for the turbulence modeling in the solid phases. The model is generalized for one gas phase and N number of solids phases to enable a realistic description of the particle-size distribution in gas/solid flow systems. Each solid phase is characterized by a diameter, form factor, density, and restitution coefficient. Simulations with one gas and two solid phases were conducted, and the computational results agreed generally well with the measurements.

Introduction

Although circulating fluidized beds (CFBs) are successfully and widely used in commercial operations, much still remains to be done due to the complexity of gas/solid flow. In order to gain better fundamental knowledge about complex multiphase flow behavior, more research is needed. Many factors influence flow behavior in a circulating fluidized bed. The inlet and exit configuration, particle size and distribution, velocity distribution of the gas as well as the solids, solid concentration, pressure and velocity fluctuations, effective viscosity, and particle properties such as cohesiveness are important factors that determine flow behavior. The hydrodynamics of gas and solids will also affect heat transfer, reaction kinetics, and catalyst activity.

To gain detailed knowledge about the flow behavior of gas/solids systems, experimental work is obviously important. Experimental research has been done for over thirty years in the area of two-phase gas/solid flow. During recent years, laser Doppler anemometry (LDA) has become one of the most commonly used experimental techniques in investigation of the flow behavior of dilute gas/solids flow systems.

Computational fluid dynamics (CFD) in multiphase flow has recently become an accepted and useful tool in modeling of gas/solids flow systems. Combined experimental and computational studies of the complex flow behavior of a circulating fluidized-bed system, such as this work, will significantly enhance the understanding of the underlying mechanisms, and provide the information to refine conservation equations and constitutive laws for gas/solids flow systems.

James et al. (1968) reported the first successful measurement with LDA. They were able to measure the velocity of a particle in air. Many scientists followed (such as Birchenough and Mason, 1976; Lee and Srinivasan, 1978; Lesinksi et al.,

Correspondence concerning this article should be addressed to V. Mathiesen.

1981; Tsuji et al., 1984; Arastoopour and Yang, 1992; Shao and Arastoopour, 1995).

Particle-size measurement using laser systems is very challenging. Dunning (1967) was the first to demonstrate that LDA could be used to estimate the particle size. He showed that a number analysis of the signal used in conjunction with the Rayleigh-Gans scattering theory would identify the particle size. Andrews and Seifert (1971) estimated the particle size by measuring the absolute value of the scattered intensity and correlating this value with a value predicted by using the Mie cross-section calculation. Farmer (1972) analyzed a method for determining particle size, number density, and velocity using a laser interferometer/velocity-meter. Using Dunning (1967) and Andrews and Seifert (1971), Farmer (1972) showed that when the fringe spacing is comparable to the particle diameter, the size can be estimated, and when the fringe spacing is much greater than the average particle diameter used, the number density can also be estimated. Depending on the optical system, the fringe spacing is generally less than 4 μm, making this technique suitable for only very small particles.

Lee and Srinivasan (1978) were the first to extract size information from peak values from a filtered anemometer. At the same time Driscoll and Mann (1978) used the broadening of the optical spectrum of scattered light to estimate the size of submicron particles. Further into the 1980s the most frequently used methods involved the two concepts of a Doppler signal: pedestals and visibility. Hishida et al. (1984), Grehan et al. (1986), and Berkelman and Renz (1989) are some of the scientists who have successfully applied these techniques.

Durst and Zare (1975) found that a linear relation exists between the diameter of a spherical particle and the Doppler signals detected at two different points in space. Almost ten years later Saffmann et al. (1984) extended the technique and presented the experimental results on bubble-size measurements. Later Bachalo and Houser (1984, 1985) measured simultaneously the droplet size and velocity in nozzle spray flow. This technique is called the ''Phase Doppler Technique'' or the ''Phase Difference Technique,'' since the phase difference between two points is related linearly to the particle size. The technique has a number of desirable features, including a very wide size range, from micron to millimeters, and good immunity to noise. A large limitation of the method is that the particles have to be smooth and spherical. However, many scientists have adopted the method in gas/solids flow as well as in liquids/solids and bubble flow. Lazaro (1991), Tadrist et al. (1993), Azario et al. (1995), Van Den Moortel et al. (1996), and Mathiesen et al. (1999) have successfully performed gas/solids measurements. Hardalupas (1988) and Jackson and Samuelsen (1988) have identified limitations and proposed some improvements to the technique.

In the early 1990s, Arastoopour and Yang (1992) modified an LDA system, including both the hardware configuration and software for data acquisition and processing. Their system could estimate the diameter of fine particles smaller than the measuring volume. The research was based on Farmer (1972), Lee and Srinivasan (1978), and the principle that the amplitude of a Doppler burst is proportional to the particle diameter. They found that this proportionality can be obtained by a calibration curve. They named the method ''Shape Discrimination Technique,'' and later Zhang and Arastoopour (1995) and Zhang et al. (1996) followed the work and successfully measured FCC, cohesion, and sand particles in the riser of a circulating fluidized bed.

For size measurements of larger particles, Shao and Arastoopour (1995) developed a technique called ''Flight Time Technique.'' The method estimates the particle diameter from the velocity and the time it takes for the particle to travel through the measuring volume. To get a good estimate of the diameter, the particle size should be larger than the width of the measuring volume, which is generally larger than 100 μm. The review chapter by Arastoopour and Shao (1997) clearly explains available LDA techniques for particle measurement.

Two different approaches are used in modeling of gas/solids systems: Lagrangian and Eulerian. The Eulerian approach, which is most commonly used, considers the solids phases as well as the gas as a continuum. The presence of each phase is described by a volume fraction. In the Lagrangian approach, the particle control volume is considered to move with the fluid. The dynamics of each particle and its interaction with the fluid are modeled. The Lagrangian approach limits the number of particles, and may not be particularly well suited yet for gas/solid flow systems like fluidized beds.

In the late 1970s, the availability of ''high speed'' computers made numerical solutions of the basic Navier-Stokes equations possible. Arastoopour and Gidaspow (1979) were the first to apply inviscid continuum equations for the particle phase to obtain desirable solids flow behavior in a one-dimensional circulating fluidized bed. Later, Tsuo and Gidaspow (1990) incorporated particle viscosities and simulated two-phase flow in a riser. They were able to describe two different flow regimes: core and annulus flow. The importance of the viscous term was obvious, and thus led the way to turbulence modeling of gas/solids systems.

Elghobashi and Abou-Arab (1983) and Chen (1985) used the well-known k-ϵ model in the carrier phase to predict the effect of the dispersed phase. This model describes the conservation of turbulent kinetic energy and its dissipation rate for the gas phase with no particle–particle interactions. Thus it is not suitable for modeling of gas/solids systems like fluidized beds.

Probably currently the best acceptable approach in modeling turbulent solids flow is ''kinetic theory of granular flow.'' This is based on the kinetic theory of nonuniform gases, as presented in the classic work of Chapman and Cowling (1970). Bagnold (1954) actually started this work as early as the 1950s. He derived a particle pressure in uniform shear flow from a simple expression for the collisional frequency of the solids. He also proposed a radial distribution function that is still frequently used.

The ''granular temperature,'' defined as proportional to the square of the fluctuating velocity, was first introduced by Jenkins and Savage (1983). Based on the kinetic theory for nonuniform gases, they solved a conservation equation for the granular temperature. To allow for inelastic collisions between two particles, they introduced a restitution coefficient. Lun et al. (1984) continued this work. Lun and Savage (1987) derived equations for granular flow, assuming mono-sized, rough, inelastic, and spherical particles.

Ahmadi and Shahinpour (1983a,b) and Ma and Ahmadi (1990a,b) used a different approach. These scientists applied

the Bhatnager–Gross–Krook (BGK) relaxation model and the Chapman Enskog iteration to solve the granular temperature. A simple model was used to account for particle/fluid interactions. The dissipation rate for the gas as well as the solid phase was given by algebraic expressions. They found reasonable agreement with experimental data.

Based on Jenkins and Savage (1983), Ding and Gidaspow (1990) extended the granular flow model starting with the Boltzmann equation for the velocity distribution of the particles. The Maxwellian velocity distribution function was used as a single particle distribution. The collisional transport consists of a binary collision, where the two particles have equal mass and size, and are smooth and inelastic. Accordingly, the model is valid for only dense gas/solids flow.

Gidaspow (1994) extended this work, and included the effect of non-Maxwellian velocity distribution. Later, Kim and Arastoopour (1995) extended the kinetic theory for cohesive particles and developed their computer code to describe the flow of gas and FCC particles in a riser of a CFB system.

With slight modifications, similar models for gas/solids flow have been developed at Telemark College (HiT-TF) by Samuelsberg and Hjertager (1996a,b), Manger (1996), and Mathiesen (1997), Morgantown Energy Technology Center (METC) by Syamlal et al. (1993); Twente University of Technology by Kuipers et al. (1993); Argonne National Laboratory by Lyczkowski and Bouillard (1989); and Babcock and Wilcox Inc., Alliance Research Center by Burge (1991). Benyahia et al. (1998) modified CFX, code for gas/solid flow systems and described two- and three-dimensional flow behavior in a riser of a circulating fluidized-bed system.

Arastoopour et al. (1982) were the first to extend one-dimensional inviscid multiphase flow equations for the flow of gas and eight different particle sizes by including particle–particle interactions in their model, and to predict particle segregation in a vertical pneumatic conveying system. Later Farrell et al. (1986) and Jenkins and Mancini (1987) extended the kinetic theory for granular flow to binary mixtures. The basic assumption was equal turbulent kinetic energy with a small correction for the individual phase temperatures. Mathiesen et al. (1997) developed a flow model based on this work and performed a simulation with one gas and three solids phases. The model predicted segregation effects fairly well and obtained good agreement with experimental data. Agarwal and Sinclair (1998) used Jenkins and Mancini's (1987) kinetic theory to describe flow of binary particle mixtures through a pneumatic conveying line.

Manger (1996) extended the kinetic theory to binary mixtures of solids with unequal granular temperatures between the phases. Both transport equations and constitutive relations for the solids phases were established. The model is valid for dilute as well as dense flow, but the relative velocities between the solids phases should not be too large. Manger (1996) did a simple test simulation in a two-dimensional channel, but no verification of the model was performed. Mathiesen et al. (1998) modified the model and simulated the flow behavior of one gas and three solids phases in a circulating fluidized bed.

In this study, experimental and computational investigations of the flow pattern of different particle sizes in the riser of a cold-flow circulating fluidized bed were conducted. The LDA technique was used to experimentally diagnose the flow behavior of gas/solids systems. Based on Yang (1991), our modified shape-discrimination technique was developed and used to estimate the particle diameter. A generalized multiphase gas/solids flow model based on Manger (1996) was developed. The model allows the user to classify the solids into several classes, referred to as different phases. The developed model was used to simulate the riser of a circulating fluidized bed. One gas and two solids phases were used in the two-dimensional simulations. Experimental and computational results were compared, analyzed, and discussed.

Experimental Measurement Technique

Laser Doppler anemometry (LDA) has become one of the most commonly used experimental tools in single- and multiphase flows. The major reasons are that LDA is a noninvasive optical technique that does not disturb the flow and has a high spatial resolution with a fast dynamic response and range. LDA was used to simultaneously measure the mean and the fluctuating velocities, and the particle diameter of the dispersed phase.

Particle velocity measurement

When two coherent Gaussian laser beams are intersecting, the intersection will cause a pattern of plane interference fringes. The intersection area forms a measuring volume. Figure 1 shows the measuring volume with fringes. The fringe spacing δ_f can be shown to be proportional to the wavelength λ and inversely proportional to half of the angle ϑ between the two incident beams.

When a particle is passing through the measuring volume, it will scatter light and the intensity

$$\delta_f = \frac{\lambda}{2\sin(\vartheta/2)} \tag{1}$$

will change according to the interference fringes (Arastoopour and Shao, 1997). The intensity variation of the scattered light or the frequency can be obtained with a photodetector. The velocity of the passing particle will be proportional to the

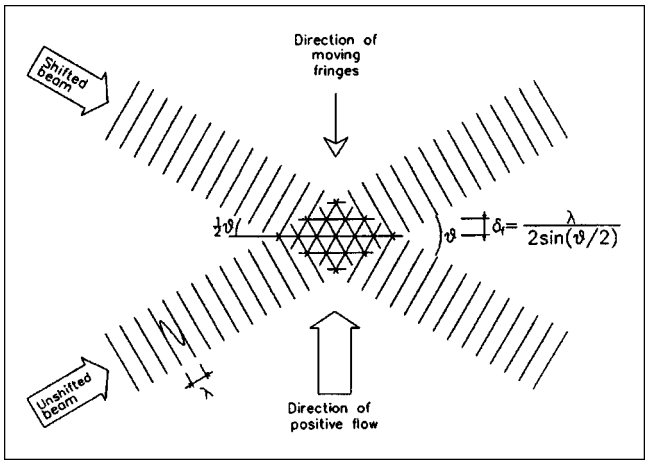

Figure 1. Overview of a measuring volume.

Doppler frequency f_D and the fringe spacing

$$v_i = f_D \delta_f = \frac{f_D \lambda}{2\sin(\vartheta/2)}, \tag{2}$$

where v_i is the absolute velocity of the particle in the direction perpendicular to the bisector of the two incident laser beams. To detect the direction of the flow, a frequency shift for one of the beams is introduced, as indicated in Figure 1. The Doppler frequency is the frequency obtained by the photodetector minus the frequency shift.

The mean velocity, V, is obtained by

$$V = \frac{1}{N_i} \sum_{i=1}^{N_i} v_i, \tag{3}$$

where N_i is the number of sampled particles. The fluctuating velocity or the root mean square (RMS) velocity, V_{RMS}, may be expressed as

$$V_{\mathrm{RMS}} = \sqrt{\frac{1}{(N_i - 1)} \sum_{i=1}^{N_i} (v_i - V)^2}. \tag{4}$$

Particle-size measurement

The Shape Discrimination Technique was established by Arastoopour and Yang (1992) and is based on knowledge about Doppler burst signals. The shape of a Doppler burst signal is determined by the size, shape, and surface properties of the particles, concentration of solids, the fluid, the path the particle takes as it passes through the focusing volume, and the optical system alignment. This study has documented that the amplitude is a function of the particle velocity as well. Hence, in a system with fixed optical parameters, one type of solid in one type of fluid at one flow condition, the maximum amplitude of a Doppler burst, A_D, or the envelope, will depend on the diameter of the particle, D_i, the particle velocity, v_i, and the path, l, that the particle is traveling through the measuring volume:

$$A_D = A_D(D_i, v_i, l). \tag{5}$$

Figure 2 shows the Doppler signals generated at different paths. For the same particle with the same velocity, the strongest signal will be generated when the particle is passing through the center of the measuring volume.

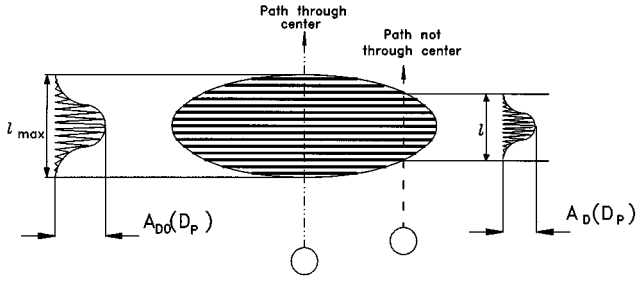

Figure 2. Doppler signal generated at different paths.

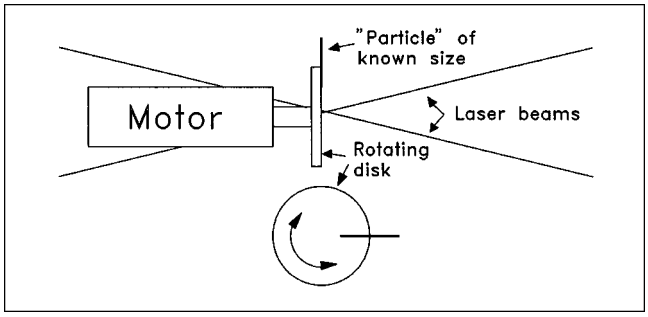

Figure 3. Experimental verification setup.

The intensity, I_D, of a Doppler burst may be rewritten according to Farmer (1972):

$$I_D = I_{D0}\left[\cosh\left(2yz\vartheta/b_0^2\right) + \cos\left(y/\delta_f\right)\right] \cdot \exp\left[\left(-2/b_0^2\right)\left(x^2 + y^2 + \left(z\frac{\vartheta}{2}\right)^2\right)\right], \tag{6}$$

where b_0 is the dimension of the measuring volume in the direction perpendicular to the optical axis. If the velocity component perpendicular to the laser-beam plane and the component parallel to the fringes are neglected, the amplitude of the Doppler burst may be rewritten as

$$A_D(D_i, v_i, l) = A_{D0}(D_i, v_i) \exp\left[-2\left(1 - \frac{l^2}{l_{\max}^2}\right)\right] \tag{7}$$

where A_{D0} is the amplitude of a Doppler burst generated by a particle that is passing through the center of the measuring volume and $l_{\max}$ is the maximum possible path length. Since effective path length and maximum possible path length are proportional to the actual peak numbers within one Doppler burst, N_{peak}, and the maximum peak numbers within one Doppler burst, $N_{\mathrm{peak,max}}$, according to Yang (1991) the preceding expression can be written as

$$A_{D0}(D_i, v_i) = A_D(D_i, v_i, l) \exp\left[2\left(1 - \frac{N_{\mathrm{peak}}^2}{N_{\mathrm{peak,max}}^2}\right)\right]. \tag{8}$$

To decide whether the velocity of a particle is influencing the size of the amplitude, a verification experiment was conducted using only one particle (with constant diameter, shape, and surface properties), air as the fluid, one optical alignment, and the same particle path. The experimental apparatus consists of a motor and a rotating disk, as shown in Figure 3. A tiny wire with known diameter is fixed on the rotating disk and mounted on a shaft of a small variable speed motor. The wire rotates with the disk and passes through the measuring volume at a specified speed, v_i. The trajectory of the particle is perpendicular to the plane forming the bisection of the two laser beams. This trajectory was manually ad-

justed to ensure that the rotating wire was passing through the center of the measuring volume.

The verification experiments were conducted at seven different particle velocities between -0.2 and 1.0 m/s. At each velocity the amplitude of the Doppler burst was measured 100 times. Figure 4 shows the mean amplitude size of the Doppler burst for two different diameters of the wire, 500 and 700 μm, respectively. The experimental apparatus was aligned in such a way that the amplitude was only a function of the diameter of the wire (particle) and the velocity:

$$A_{D0} = A_{D0}(D_i, v_i). \tag{9}$$

As indicated in Figure 4, the amplitude of the Doppler burst for a diameter of 500 μm can be expressed as

$$A_{D0}(v_i) = -0.27v_i^3 + 0.26v_i^2 + 0.01v_i + 0.04, \tag{10}$$

and with a diameter of 700 μm as

$$A_{D0}(v_i) = 1.78\left[-0.27v_i^3 + 0.26v_i^2 + 0.01v_i + 0.04\right]. \tag{11}$$

A generalized empirical relation between the amplitude of the Doppler burst and the velocity of the particles can then be expressed as

$$A_{D0}(D_i, v_i) \propto A_{D0}(D_i)\left[-0.27v_i^3 + 0.26v_i^2 + 0.01v_i + 0.04\right], \tag{12}$$

when -0.2 m/s $< v_i <$ 1.0 m/s. By combining Eq. 8 and Eq. 12, an expression for the amplitude as a function of the diameter may be obtained:

$$A_{D0}(D_i) \propto A_D(D_i, v_i, l)\frac{\exp\left[2\left(1 - \dfrac{N_{\text{peak}}^2}{N_{\text{peak, max}}^2}\right)\right]}{\left[-0.27v_i^3 + 0.26v_i^2 + 0.01v_i + 0.04\right]}. \tag{13}$$

The maximum amplitude of the Doppler burst calculated by Eq. 13 will be proportional to the size of the particle that causes the burst. A calibration curve for the amplitude of the Doppler burst vs. particle diameter cannot be obtained theoretically. Hence the amplitude to the diameter transformation of the particles should be determined by an experimentally verified calibration procedure. The experimental calibration curve can be obtained using the following procedure:

1. Measure the particle-size distribution by using a well-recognized particle-size instrument and generate the particle diameter vs. accumulative percentage.
2. Mount the experimental equipment and align the LDA optical system.
3. Specify the flow condition; calibration must be done for each flow condition.
4. Record a large number of amplitudes at different radial locations.

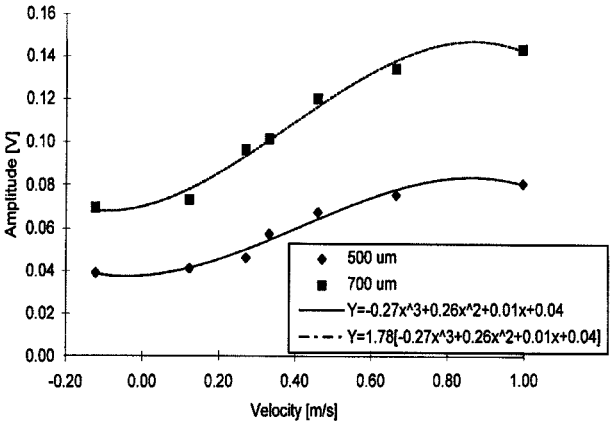

Figure 4. Amplitude as a function of particle velocity.

5. Calculate the maximum amplitudes (envelope) of the individual Doppler bursts by using Eq. 13.
6. Correct the number of amplitudes for area and time.
7. Develop the calibration curve by comparing the particle-size and amplitude-size distribution. The calibration curve is used to estimate the particle diameter.

When a given number of particles have been estimated, the mean number particle diameter may be obtained:

$$D_{\text{Number}} = \frac{1}{N_i}\sum_{i=1}^{N_i} D_i. \tag{14}$$

Using this technique, the noise must be discriminated, since the amplitude is very sensitive. The high- and low-frequency noise can be discriminated by using a signal processor. The possible noise in the receiving Doppler signal due to electronic devices is discriminated using time and periodic criteria. A reasonable Doppler burst should be longer than a minimum time duration $\tau_{\min}$:

$$\tau_{\min} \le \tau_i, \tag{15}$$

where τ_i is the time duration for the Doppler burst signal. A perfect Doppler signal should be oscillating with the same period, at constant frequency. The standard deviation of the oscillating period in the Doppler burst should be less than a critical level:

$$\frac{\sqrt{\dfrac{1}{\left(N_{\text{peak}} - 1\right)}\displaystyle\sum_{k=1}^{N_{\text{peak}}}\left(\Delta\tau_k - \overline{\Delta\tau}\right)^2}}{\overline{\Delta\tau}} \le \text{critical level}, \tag{16}$$

where $\Delta\tau_k$ is the kth period and $\overline{\Delta\tau}$ is the average period in the Doppler burst. In this experimental work, the critical level is set equal to 0.5.

Fluid Dynamic Model

A multiphase computational fluid dynamics (CFD) model for turbulent gas/solids flow was developed and presented.

In our model, we used M phases, one gas, and N number of solids phases to describe realistic particle-size distributions. Each solid phase was defined by diameter, form factor, density, and restitution coefficient. The model uses a Eulerian description of the phases, which considers the gas as well as each solid phase as a continuum medium. The presence of each phase was described by a volume fraction, varying from zero to one. No mass transfer was allowed between the phases. The drag force in the momentum equation and the product of drag force and granular temperature in the particle turbulent kinetic energy equation were the only interfacial terms between the gas and particle phase that were used in our model. The effect of gas turbulence on the particle fluctuation as well as the effect of gas on the constitutive relations of the particulate phases were neglected. Since small-size particles such as FCC were used in our simulation, this assumption can be considered as the major limitation of our model.

The laws of conservation of mass, momentum, and energy were individually satisfied for each phase. The dependent variables, namely, volume fraction and the three velocity components were solved for each phase. All the phases share a fluid pressure. A granular temperature equation (defined as one-third times the fluctuation velocity squared) for each solids phase was solved also. No turbulence equation for the gas phase was considered, but an effective gas viscosity was estimated.

To obtain governing flow equations for the solid phases, the Boltzmann equation was used with a given distribution function for the instantaneous velocity of the particles. By multiplying the Boltzmann equation with a quantity such as mass or momentum, and integrating over the velocity space, the transport equations were obtained (Chapman and Cowling, 1970). A complete derivation of the equations for gas/solids flow was done by Gidaspow (1994). The particles were assumed inelastic, smooth, and spherical. Particle rotation was neglected. Furthermore, the constitutive relations to close the transport equations were also provided using this method. These constitutive equations specify how the physical parameters of the phases interact with each other.

Manger (1996) provided an extension to binary mixtures of particulate materials and derived transport equations for each solids phase. His approach involved kinetic theory for binary granular mixtures with unequal temperatures between the phases. The constitutive equations were based on the interactions of the fluctuating and the mean motion of the particles. The shear stresses were considered as the sum of a collisional and a kinetic component. The pressure of the solid phases, which includes both kinetic and collisional pressures, was determined from an equation of state similar to the van der Waals equation of state for gases, based on the coefficient of restitution and the radial distribution function concepts. The radial distribution function is an expression for a probability of collisions, and is near one when the flow is dilute and becomes infinite when the flow is so dense that motion is impossible. The shear viscosities for dilute and dense flow are proportional to the mean free path times an oscillation velocity times particle density. The coupling between the various particle phases is through particle pressures, binary radial distribution functions, particle collisions, and conductivities.

The mathematical model was incorporated in the CFD model, FLOTRACS-MP-3D, with the following governing constitutive equations. A detailed description of the multiphase gas/solids model is given by Mathiesen (1997), whereas Mathiesen et al. (1999) discuss the consistency of the multiphase gas/solid flow model in detail.

Continuity equations

The continuity equation for phase m is given by

$$\frac{\partial}{\partial t}\left(\beta_v \epsilon_m \rho_m\right) + \frac{\partial}{\partial x_i}\left(\beta_i \epsilon_m \rho_m U_{i,m}\right) = 0, \qquad (17)$$

where ϵ, ρ, and U_i are volume fraction, density, and the ith direction velocity component, respectively; β_v is volume porosity; and β_i is the area porosity in the ith direction. No mass transfer is allowed between the phases.

Momentum equations

The momentum equations in the j-direction for phase m can be expressed as

$$\begin{aligned}\frac{\partial}{\partial t}\left(\beta_v \epsilon_m \rho_m U_{j,m}\right) + \frac{\partial}{\partial x_i}\left(\beta_i \epsilon_m \rho_m U_{i,m} U_{j,m}\right) \\ = -\left(\beta_v \epsilon_m\right)\frac{\partial P}{\partial x_j} + \frac{\partial}{\partial x_i}\left(\beta_i \Pi_{ij,m}\right) + \beta_v \epsilon_m \rho_m g_j \\ + \beta_v \sum_{k=1, k\neq m}^{M} \Phi_{mk}\left(U_{j,k} + U_{j,m}\right), \qquad (18)\end{aligned}$$

where P and g_i are fluid pressure and j-direction component of gravity, respectively; and Φ_{mk} is the drag coefficient between the phases m and k.

For the gas phase, g the stress tensor $\Pi_{ij,g}$ is given by

$$\Pi_{ij,g} = \mu_{\text{eff},g}\left[\left(\frac{\partial U_j}{\partial x_i} + \frac{\partial U_i}{\partial x_j}\right) - \frac{2}{3}\delta_{ij}\frac{\partial U_k}{\partial x_k}\right]_g, \qquad (19)$$

where δ_{ij} is the Kroenecker delta. The gas-phase turbulence was modeled by the subgrid scale (SGS) model proposed by Deardorff (1971), and thus the effective viscosity, $\mu_{\text{eff},g}$, was estimated as

$$\begin{aligned}\mu_{\text{eff},g} &= \epsilon_g\left(\mu_{\text{lam},g} + \mu_{\text{turb},g}\right) \\ &= \epsilon_g \mu_{\text{lam},g} + \epsilon_g \rho_g \left(c_t \Delta\right)^2 \sqrt{S_{ij,g} : S_{ij,g}}\end{aligned}$$

$$\Delta = \sqrt[3]{\Delta x \Delta y \Delta z} \quad \text{and} \quad S_{ij,g} = \frac{1}{2}\left[\frac{\partial U_j}{\partial x_i} + \frac{\partial U_i}{\partial x_j}\right]_g. \qquad (20)$$

The constant turbulence parameter, c_t, is estimated to 0.079 by using renormalization group (RNG) theory (Yakhot and Orszag, 1986).

The total stress tensor $\Pi_{ij,s}$ for each solid phase, s, is

$$\Pi_{ij,s} = -P_s\delta_{ij} + \xi_s\delta_{ij}\frac{\partial U_{k,s}}{\partial x_k} + \mu_s\left[\left(\frac{\partial U_j}{\partial x_i} + \frac{\partial U_i}{\partial x_j}\right) - \frac{2}{3}\delta_{ij}\frac{\partial U_k}{\partial x_k}\right]_s, \tag{21}$$

where the solid phase pressure, P_s, consists of a collisional and a kinetic term:

$$P_s = \sum_{n=1}^{N} P_{C,sn} + \epsilon_s\rho_s\theta_s, \tag{22}$$

where $P_{C,sn}$ is the pressure caused by collisions between the solids phases s and n, and has the expression:

$$P_{C,sn} = \frac{\pi}{3}(1+e_{sn})d_{sn}^3 g_{sn} n_s n_n \left\{\frac{m_0\theta_s\theta_n}{((m_s/m_n)\theta_s + (m_n/m_s)\theta_n)}\right\} \times \left\{\frac{(m_0/m_s)^2\theta_s\theta_n}{\left(\theta_s + (m_n/m_s)^2\theta_n\right)(\theta_s+\theta_n)}\right\}^{3/2}$$

$$e_{sn} = \frac{1}{2}(e_s + e_n) \quad \text{and} \quad d_{sn} = \frac{1}{2}(d_s + d_n) \quad \text{and} \quad m_0 = m_s + m_n, \tag{23}$$

where e, d, n, and m are the coefficient of restitution, diameter of the particle, number of particles, and mass of a particle, respectively. The coefficient of restitution is unity for fully elastic and zero for plastic collisions. By using the assumption of spherical particles, number of particles and mass of a particle are:

$$n_s = \frac{6\epsilon_s}{\pi d_s^3} \quad \text{and} \quad m_s = \frac{\pi d_s^3\rho_s}{6}. \tag{24}$$

The radial distribution function, g_{sn}, is near one when the flow is dilute and becomes infinite when the flow is so dense that motion is impossible. Based on the single solids phase model given implicitly by Bagnold (1954), a new binary radial distribution function was proposed:

$$g_0 = \left\{1 - \left(\frac{1-\epsilon_g}{\epsilon_{s,\max}}\right)^{1/3}\right\}^{-1}$$

$$g_{sn} = \frac{N}{2}\frac{g_0}{(1-\epsilon_g)}(\epsilon_s + \epsilon_n), \tag{25}$$

where $\epsilon_{s,\max}$ is the maximum total volume fraction of solids.

The solid phases bulk viscosity can be written as

$$\xi_s = \sum_{n=1}^{N} P_{C,sn}\frac{d_{sn}}{3}(\theta_s + (m_n/m_s)\theta_n) \times \sqrt{\frac{2}{\pi\theta_s\theta_n\left[\theta_s + (m_n/m_s)^2\theta_n\right]}}, \tag{26}$$

whereas the solid phases shear viscosity consists of a collisional term:

$$\mu_{\text{col},s} = \sum_{n=1}^{N} P_{C,sn}\frac{d_{sn}}{5}(\theta_s + (m_n/m_s)\theta_n) \times \sqrt{\frac{2}{\pi\theta_s\theta_n\left(\theta_s + (m_n/m_s)^2\theta_n\right)}} \tag{27}$$

and a kinetic term

$$\mu_{\text{kin},s} = \frac{2\mu_{\text{dil},s}}{\frac{1}{N}\sum_{n=1}^{N}(1+e_{sn})g_{sn}}\left\{1 + \frac{4}{5}\sum_{n=1}^{N} g_{sn}\epsilon_n(1+e_{sn})\right\}^2, \tag{28}$$

where

$$\mu_{\text{dil},s} = \frac{15}{8d_s^3}\epsilon_s l_s\sqrt{\frac{2m_s\theta_{s,\text{av}}}{\pi}}$$

$$l_s = \frac{1}{6\sqrt{2}}\frac{d_s}{\epsilon_s}. \tag{29}$$

To ensure that the dilute viscosity is finite as the volume fraction of solids approaches zero, the mean free path, l_s, is limited by a characteristic dimension. The average granular temperature $\theta_{s,\text{av}}$ was obtained from

$$\theta_{s,\text{av}} = \frac{2m_s\theta_s}{\left\{\sum_{n=1}^{N}\left(\frac{n_n}{n_s}\right)\left(\frac{d_{sn}}{d_s}\right)^2\sqrt{\frac{(m_0/m_s)^2\theta_n}{\left(\theta_s + (m_n/m_s)^2\theta_n\right)}}\,S^{3/2}\right\}^2}$$

$$S = \frac{(m_0/m_s)^2\theta_s\theta_n}{\left(\theta_s + (m_n/m_s)^2\theta_n\right)(\theta_s+\theta_n)}. \tag{30}$$

For $\epsilon_g \le 0.8$, the gas/solids drag coefficients were based on the Ergun (1952) equation:

$$\Phi_{sg} = 150\frac{\epsilon_s(1-\epsilon_g)\mu_{\text{lam},g}}{\epsilon_g(\psi_s d_s)^2} + 1.75\frac{\epsilon_s\rho_g|u_g - u_s|}{\psi_s d_s}, \tag{31}$$

where ψ_s is the form factor, which is unity for spheres and between zero and one for all other particles. For $\epsilon_g > 0.8$, the drag coefficients were based on the work by Wen and Yu (1966) and Rowe (1961):

$$\Phi_{sg} = \frac{3}{4}C_d\frac{\epsilon_s\epsilon_g\rho_g|u_g - u_s|}{\psi_s d_s}\epsilon_g^{-2.65}$$

$$C_d = \frac{24}{Re_s}(1 + 0.15\,Re^{0.687}) \quad \text{for } Re_s \le 1{,}000$$

$$C_d = 0.44 \quad \text{for } Re_s > 1{,}000$$

$$Re_s = \frac{d_s\rho_g\epsilon_g|u_g - u_s|}{\mu_{\text{lam},g}}. \tag{32}$$

In this study, ϵ_g was less than 0.8. The particle/particle drag coefficients were expressed as

$$\Phi_{sn} = \beta_v P_{C,sn}\left\{\frac{3}{d_{sn}}\sqrt{\frac{2\left(m_s^2\theta_s + m_n^2\theta_n\right)}{\pi m_0^2\theta_s\theta_n}} + \frac{1}{|u_n - u_s|}\right.$$
$$\left.\times\left[\nabla\left|\ln\frac{\epsilon_s}{\epsilon_n}\right| + \frac{\theta_s\theta_n}{\theta_s+\theta_n}\left|\frac{\nabla\theta_n}{\theta_n^2} - \frac{\nabla\theta_s}{\theta_s^2}\right| + 3\nabla\left|\frac{\ln(m_n\theta_n)}{\ln(m_s\theta_s)}\right|\right]\right\}. \quad (33)$$

Turbulent kinetic energy equations

A turbulent kinetic energy equation or a granular temperature equation was solved for each solid phase:

$$\frac{3}{2}\left[\frac{\partial}{\partial t}(\beta_v\epsilon_s\rho_s\theta_s) + \frac{\partial}{\partial x_i}(\beta_i\epsilon_s\rho_s U_{i,s}\theta_s)\right] = \beta_v\left(\prod_{ij,s}:\frac{\partial U_{j,s}}{\partial x_i}\right)$$
$$+\frac{\partial}{\partial x_i}\left(\beta_i\kappa_s\frac{\partial\theta_s}{\partial x_i}\right) - \beta_v\gamma_s - 3\beta_v\Phi_{sg}\theta_s. \quad (34)$$

The terms on the right side of the equation represent production due to shear, diffusive transport of granular temperature, dissipation due to inelastic collisions, and dissipation due to fluid friction. A corresponding production term due to fluctuations in drag has been assumed negligible.

The conductivity of granular temperature, κ_s, and the dissipation due to inelastic collisions, γ_s, are determined from the kinetic theory for granular flow. The conductivity is given by a dilute and a dense part as

$$\kappa_s = \frac{2\kappa_{\mathrm{dil},s}}{\frac{1}{N}\sum_{n=1}^{N}(1+e_{sn})g_{sn}}\left\{1 + \frac{6}{5}\sum_{n=1}^{N} g_{sn}\epsilon_n(1+\epsilon_{sn})\right\}^2$$
$$+2\epsilon_s\rho_s d_s\sqrt{\frac{\theta_s}{\pi}}\sum_{n=1}^{N}\epsilon_n g_{sn}(1+e_{sn})$$

$$\kappa_{\mathrm{dil},s} = \frac{225}{32}\epsilon_s l_s\sqrt{\frac{2m_s\theta_{s,\mathrm{av}}}{\pi}}. \quad (35)$$

The dissipation of the turbulent kinetic energy due to particle collisions is given by

$$\gamma_s = \sum_{n=1}^{N}\frac{3}{4}P_{C,sn}\frac{(1-e_{sn})}{d_{sn}}$$
$$\times\left[4\sqrt{\frac{2\theta_s\theta_n}{\pi\left[(m_s/m_o)^2\theta_s + (m_n/m_0)^2\theta_n\right]}}\right.$$
$$\left. - d_{sn}\left(\frac{(m_s/m_0)\theta_s + (m_n/m_0)\theta_n}{(m_s/m_0)^2\theta_s + (m_n/m_0)^2\theta_n}\right)\frac{\partial U_{k,s}}{\partial x_k}\right]. \quad (36)$$

Experimental Setup

An experimental study of a circulating fluidized bed with FCC catalysts as the dispersed phase was conducted. The work was carried out at the Illinois Institute of Technology (IIT), Department of Chemical and Environmental Engineering. The circulating fluidized-bed system was first used by Yang (1991). In this work, slight modifications of the circulating fluidized-bed system and the LDA system were performed.

Circulating fluidized bed

A sketch of the circulating fluidized-bed system is shown in Figure 5. The internal diameter of the clear PVC riser is 0.0508 m (2 in.), the height of the riser is 2.75 m (9 ft). The test section is located 1.12 m over the elbow inlet, where a pair of optical glass windows is mounted to ensure a good optical signal. At the top of the riser, the suspended particles enter a two-stage cyclone where they are recycled back to the riser via a return loop. The gas inlet consists of air filters, a pressure regulator, and a flowmeter. The air has a pressure of about 1 bar and ambient temperature at the inlet.

The FCC catalysts have a density of 1,700 kg/m^3. The particle-size distribution is very wide with particles ranging from 11 to 180 μm. The effective number mean and Sauter mean diameter are approximately 27 and 55 μm, respectively. According to the classification of Geldart (1973), the FCC catalysts are typically group A, aeratable particles. Four different flow conditions were studied. Two superficial gas velocities were used—0.7 and 1.4 m/s—each with 100- and 400-g loading of solids, respectively. This gave an approximate concentration of solids in the circulating fluidized bed of 0.5 and 2%, respectively.

Laser Doppler anemometry

The measurements were performed with a helium–neon laser with a power of 15 mW at a wavelength of 638.2 nm, delivered by TSI. The optical system is aligned on axis in forward scatter modus. Transmitting and receiving lenses both have a focal length of 250 mm. The width and height of the measuring volume are 0.18 and 1.2 mm, respectively.

An oscilloscope was used to record the Doppler signals, which were transferred to a computer. The data acquisition and processing software developed by Yang (1991) were slightly modified. The measurements were conducted at 13 different locations from the center line of the riser toward the wall, in a direction perpendicular to the plane shown in Figure 5. Mean velocity, RMS velocity, and particle diameter were simultaneously measured. The Shape Discrimination Technique was used to estimate the diameter of the particles. The particle mixture was divided into two groups: sizes less than and sizes larger than the number mean diameter. Mean and RMS velocity profiles were measured for each particle group.

Numerical Flow Conditions

The riser section of the circulating fluidized bed was modeled and simulated in a two-dimensional Cartesian coordinate system. In order to study the influence of the grid resolution, the case with a superficial gas velocity of 0.7 m/s and 0.1 kg of solids was simulated with three different grid resolutions. Uniform grids with 14×62, 26×122, and an expanded grid with 18×82 grid nodes were used in the com-

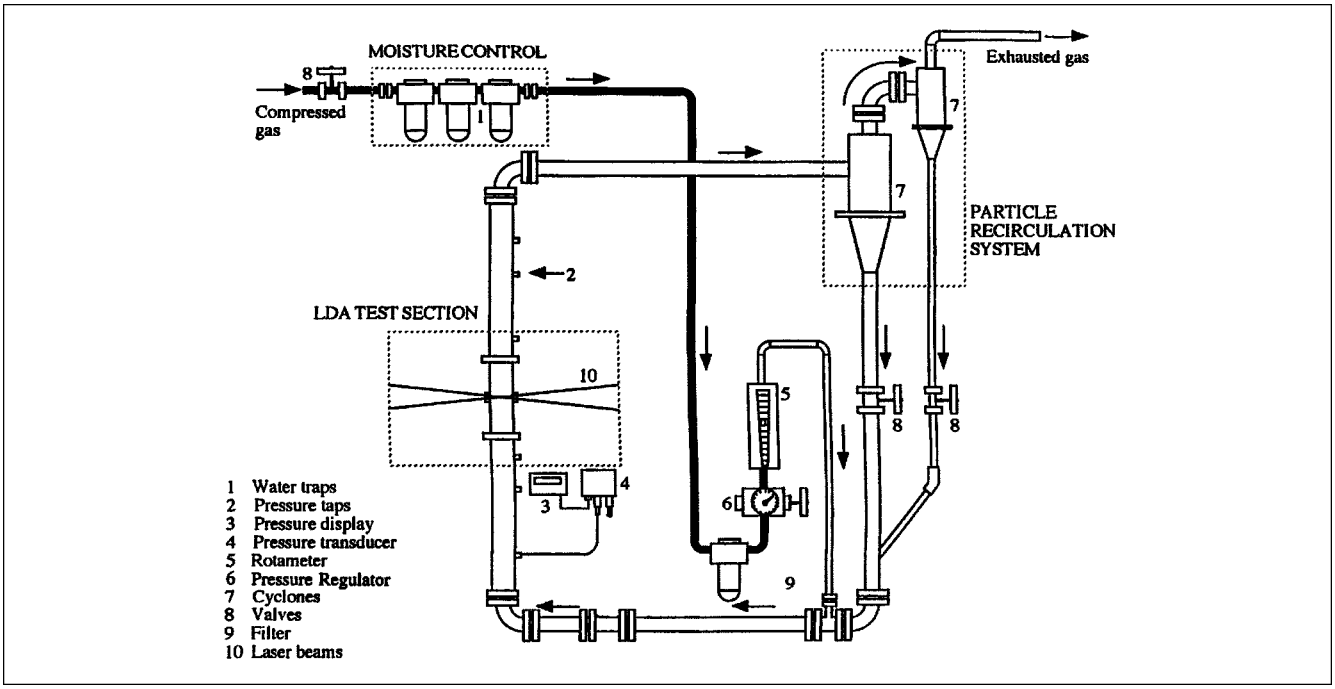

Figure 5. Circulating fluidized-bed system.

parison. The simulated velocity profiles of different phases were compared. Figure 6 shows the influence of the grid resolution on the particle velocity profile for solid phase I. Based on the results, the expanded grid with 18×82 grid nodes was assumed to be adequate for these simulations. The selected calculation domain with grid nodes is given in Figure 7. A uniform grid was used in the axial direction, whereas a nonuniform grid spacing was used in the radial direction.

The diameter of a spherical particle is uniquely defined. When dealing with nonspherical particles such as FCC catalysts, the definition of the particle diameter is more doubtful. Kunii and Levenspiel (1991) defined an effective diameter, d_{eff}, that is proportional to the form of the particle ψ and the diameter of a sphere having the same volume as the particle:

$$d_{\text{eff}} = \psi d_{\text{sphere}}, \tag{37}$$

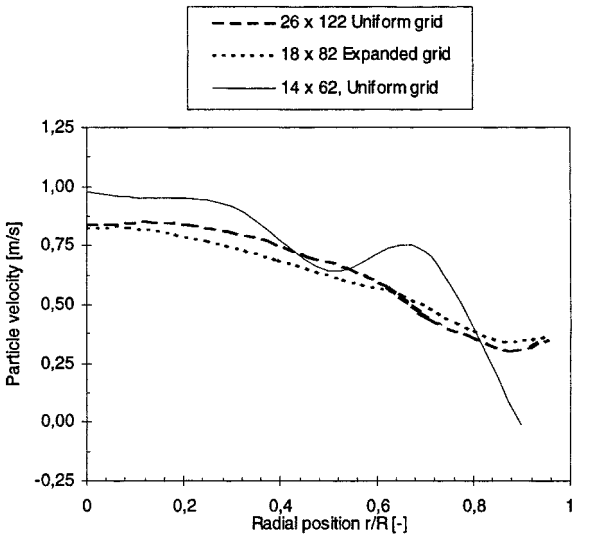

Figure 6. Grid refinement influence on particle velocities.

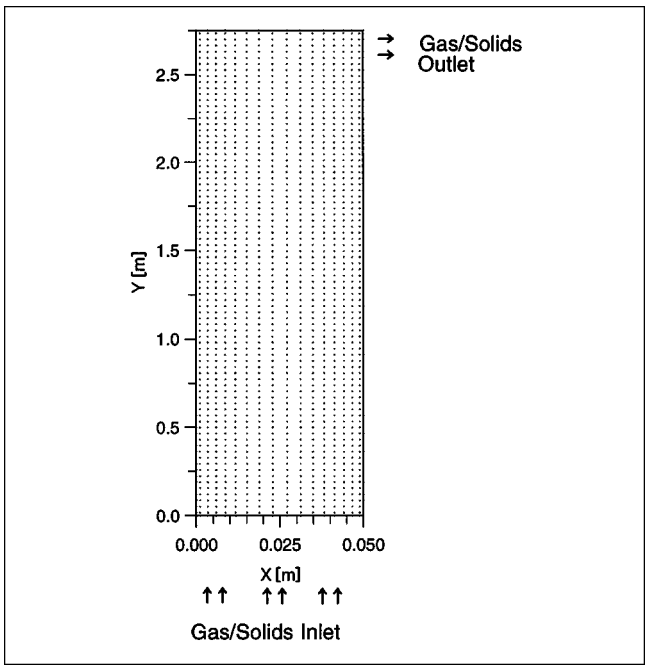

Figure 7. Circulation domain with grid nodes.

where the form factor (sphericity) is defined as

$$\psi = \frac{\text{surface of sphere}}{\text{surface of particle}}. \qquad (38)$$

The diameter of a sphere d_{sphere} is the most correct diameter to use in the kinetic theory for granular flow as well as in the calculation of drag terms and Reynolds number. The initial particle-size distribution was obtained using the Microtrac Particle Size Analyzer. This measurement technique was based on absorption or diffraction of the scattered light intensity from a laser light source. The technique measures the projected area diameter, and this projected diameter will be approximately the same as the effective diameter in Eq. 37. The Shape Discrimination Technique uses the particle diameter obtained by the Microtrac Particle Size Analyzer to make a calibration curve, and hence this diameter is an effective diameter as well. Kunii and Levenspiel (1991) calculated sphericity of particles and suggested a form factor of 0.625 as typical for catalyst solids. This value was adopted as the form factor of the FCC catalysts in the simulations.

The real particle-size distribution was modeled by using two solids phases. Ten volume percent of the solids were assumed to have an effective diameter of 25 μm, whereas the other 90% have a diameter of 60 μm. This gives an approximately correct Sauter mean diameter. Thus the equivalent diameters of the spheres were 40 and 96 μm for the two solids phases, respectively. The particle restitution coefficients were assumed to be 0.99.

The riser was initially filled with a bed of solid particles, with a total solids volume fraction of 0.50. The initial bed height was 0.03 and 0.12 m for 100 and 400 g of solids, respectively. The two solids phases were perfectly mixed.

One-dimensional plug flow for the gas phase was assumed at the inlet. To ensure that the overall continuity condition was satisfied, the gas-phase velocities were calculated from total mass balance at the outlet. The inlet solids flux was the same as the outlet solids flux, hence a constant overall concentration in the riser was ensured.

At the walls, the no-slip condition was used for the gas phase. The relation for the solids velocity gradients at the wall was based on the microscopic model for particle–wall collisions (Sinclair and Jackson, 1989). The rate of transfer of momentum to the wall by particle collisions was given by the product of the average collision frequency of each adjacent particle with the wall, the averaged momentum transfer per collision, and the averaged number of particles adjacent to unit area of the surface:

$$\tau_w = \mu_s \frac{\partial U_{j,s}}{\partial x_i} = \frac{\epsilon_s}{\epsilon_{s,\max}} \frac{\pi}{6} \rho_s \omega_s \sqrt{3\theta_s}\, U_{j,s}\, g_{ss,w}, \qquad (39)$$

where ω is a specularity factor, whose value varies between zero for a completely specular collision and unity when particles are scattered diffusively. Sinclair and Jackson (1989) also gave an expression for the turbulent kinetic energy flux at the wall as the turbulence production minus the rate of dissipation per unit area, given by

$$q_w = \frac{\epsilon_s(1-\epsilon_g)}{\epsilon_{s,\max}} g_{ss,w} \pi\sqrt{3}\, \rho_s \left[\frac{\omega_s}{6} \sqrt{\theta_s}\, U_{j,s}^2 - \frac{1}{4}(1-e_{sw}^2)\theta_s \sqrt{\theta_s} \right]. \qquad (40)$$

The specularity factor and particle-wall restitution coefficient were 0.5 and 0.9, respectively. A zero-gradient condition was used for the volume fraction and pressure equations.

The simulations were conducted for 15 s real time. The time-averaged results were obtained from the last 5 s of each simulation.

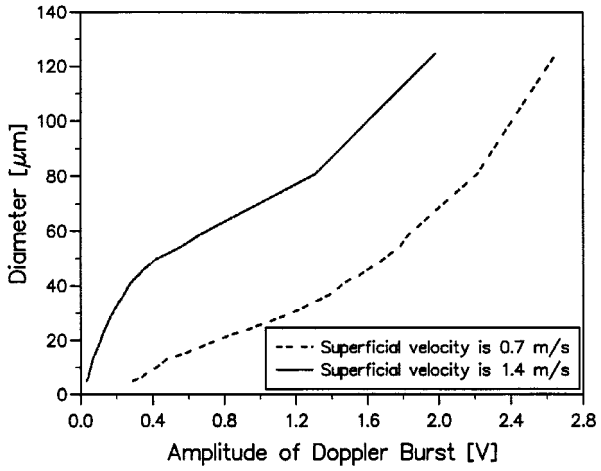

Figure 8. Calibration curves for 0.1 kg of solids.

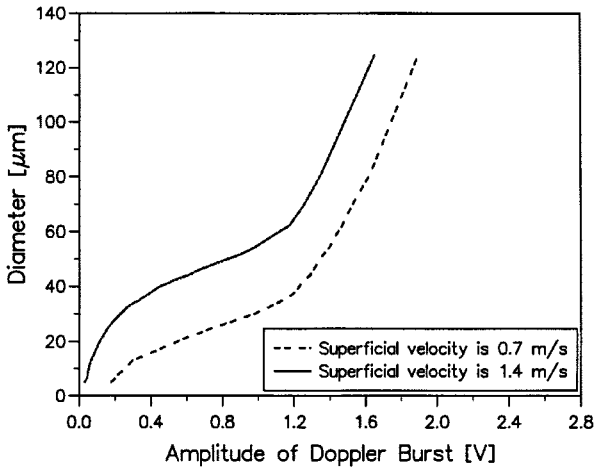

Figure 9. Calibration curves for 0.1 kg of solids.

Experimental and Numerical Results

Particle diameter calibration curves

When the Shape Discrimination Technique is used to estimate the particle diameter, a calibration curve must be obtained for each flow condition. The calibration curves are presented in Figures 8 and 9. All the calibration curves showed similar shapes, which indicates that the particle-size distribution in the test section is similar for all flow conditions. Hence there is no significant axial segregation in the

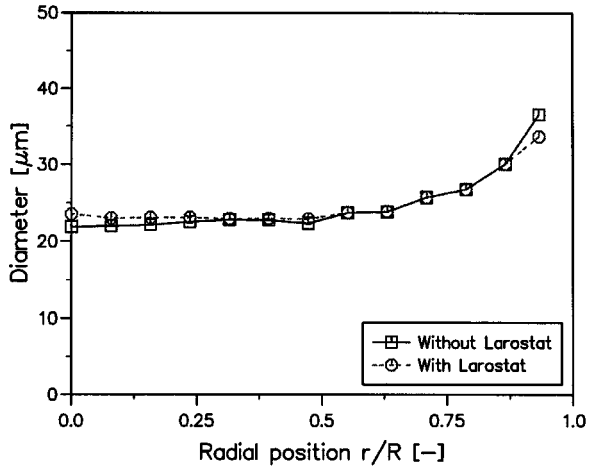

Figure 10. Measured particle diameter profiles with and without Larostat particles.

riser. The calibration curves also demonstrated the importance of making a new calibration curve for each flow condition. The main reason for the differences in the calibration curves is the variation of local particle concentrations in the test section at different flow conditions. The test section was located 1.12 m above the inlet. For a low gas velocity of 0.7 m/s, a nonuniform axial concentration distribution of the solids occurred. When the superficial gas velocity increases to 1.4 m/s, the axial solid concentration distribution is more uniform and hence results in a higher solids concentration in the test section. The calibration curves confirmed that the amplitude of a Doppler burst is a function of the solid concentration. When the concentration of solids increases, the slope of the calibration curve will increase as well. The amplitude of the Doppler burst becomes more independent of the particle diameter when the solid concentration increases. Since a wide-range amplitude distribution is desirable for calibration curves at different solid concentration, the Shape Discrimination Technique is best suited for very dilute gas/solids flow systems.

The calibration curves for the particle-size measurements are based upon the fundamental assumption that there is no agglomeration or axial segregation in the system. A superficial gas velocity of 0.7 and 1.4 m/s was assumed to be sufficient to minimize axial segregation. In a dilute gas/solids flow system, agglomeration increases with the concentration of particles and/or the superficial velocity of the continuous phase. Among these flow conditions, most agglomerates were probably obtained with 400 g of solids and high superficial gas velocity. The agglomeration was mainly caused by electrostatic effects (Zhang et al., 1996). Larostat particles eliminate electrostatic forces and, in turn, agglomeration. Thus two experiments using 400 g of solids with a superficial gas velocity of 1.4 m/s, one without Larostat and one with 1% Larostat particles mixed with the FCC were conducted. Figure 10 shows a comparison of the measured number averaged particle diameter along the radial direction for both cases. The experimental results obtained with Larostat particles showed slightly higher particle diameters at the center of the riser and lower particle diameters near the wall in comparison with the run using no Larostat particles. The maximum difference between the local mean particle diameters in the two cases is about 2.5 μm. Hence, no significant agglomeration occurred in the gas/solids flow cases that were considered in this study.

Particle diameter profiles

In Figure 11 the computed and measured numbers represent averaged diameter profiles at 1.4 m/s gas superficial gas velocity. The most interesting observation in the measured particle diameter profiles was the significant difference in mean diameter between particles at the center of the riser and those near the wall. The radial particle diameter gradient seems to increase with decreasing concentration of solids and seems to be almost independent of the gas velocity in the range in which our experiments were conducted. This phenomenon may be explained by the fact that smaller particles will follow the gas more effectively than larger ones. Larger particles will not follow the gas effectively and start accumulating, particularly at the wall region where the gas velocity is low.

Our predicted mean particle diameter profiles are independent of radial location. The discrepancies were observed in comparison with the experimental data, where the particle diameter increases with radial location with maximum average particle size at the wall region. Our multiphase gas/solids flow model did not capture the radial segregation by size, although the overall mean diameter obtained was approximately the same as the one measured experimentally. We believe that a reason for the discrepancies between the experimental data and the simulation is that in simulation, we considered only two sizes of particles (25 and 60 μm). The particle size in any location could not be lower than 25 μm or higher than 60 μm, while experimentally we have particle sizes ranging from 11 μm to 180 μm. Future simulations should include more particle phases, which in turn require much higher computational time.

Figure 12 shows the volume fraction of the solids phases obtained at a superficial gas velocity, and solid loading of 0.7 m/s and 0.1 kg. No volume fraction measurements were performed, but the computed volume fraction distribution has

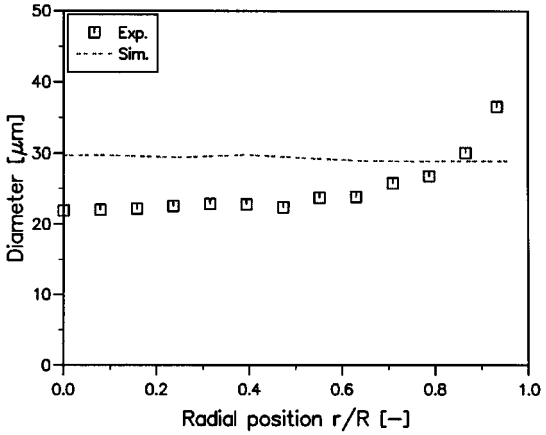

Figure 11. Mean particle diameter profiles, V_{sup} = 1.4 m/s, 0.4 kg solids.

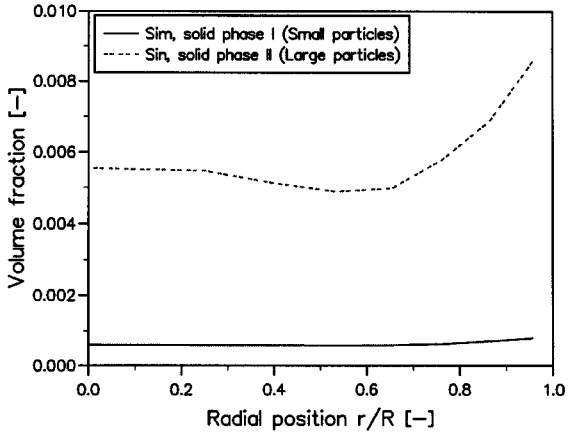

Figure 12. Volume fraction profiles, $V_{sup} = 0.7$ m/s, 0.1 kg solids.

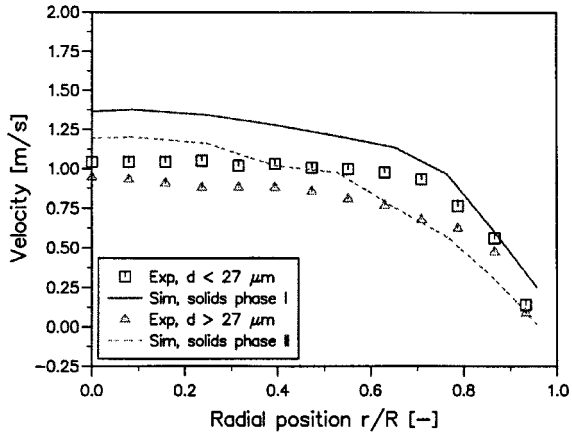

Figure 14. Particle velocity profiles, $V_{sup} = 1.4$ m/s, 0.1 kg solids.

an expected form, dilute in the center of the riser and dense in the wall region, behavior that is typical for dilute gas/solids flow. For both phases the concentration of solids increases from the center of the riser toward the wall, but at a much higher rate for the largest particles: solid phase II.

Particle velocity profiles

The measured and computed particle velocity profiles are presented in Figures 13, 14, 15, and 16. The particles are divided into two groups: particles with diameter less than 27 μm and particles with diameter larger than 27 μm, corresponding to the two solid phases.

Typical core-annulus flow behavior for the particulate phases was observed for all flow conditions. The experimental results showed that in the central part of the riser, the particles flow upward with an almost constant velocity. In the wall region, the particle velocity decreases continuously from the core toward the wall. Close to the wall, a low particle velocity and, in some cases, reversal flow of particles were observed.

Our numerical and experimental results showed a relative velocity between particles of different sizes. The calculated relative velocity between the two groups of particles remained almost constant across the riser. Our experimental data showed that when the superficial gas velocity increases, the relative velocity between the particle groups decreases slightly. This could be due to an increase in particle collisions and more chaotic flow at higher gas velocities. At higher solids loadings and higher velocities, the particles show a more flat solid velocity profile and, in some cases (such as high solids loading and high gas velocity), the maximum velocity deviates slightly from the center of the riser.

Although discrepancies were observed between measured and computed velocity profiles, the simulations showed a similar flow behavior. A typical core-annulus flow was computed with upflow of particles in the central part of the riser and downflow of particles near the wall. The predicted relative velocities are of the right order of magnitude as experimental measurements, although calculated velocity was higher than experimental data in the annulus region.

The discrepancies in the velocity profiles can be explained by the differences in actual and simulated geometry as well as different particle-size distribution. Two basic simplifications of the geometry were done in the simulations. Only the

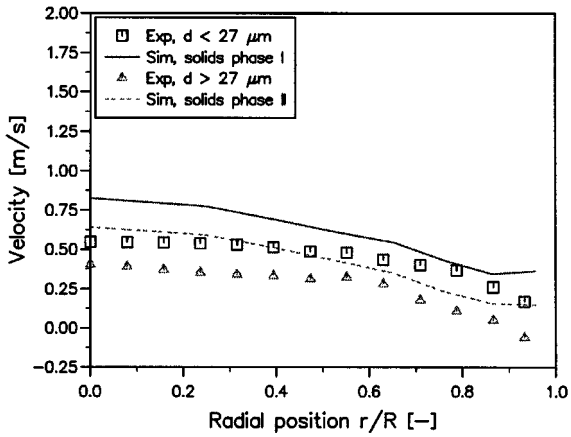

Figure 13. Particle velocity profiles, $V_{sup} = 0.7$ m/s, 0.1 kg solids.

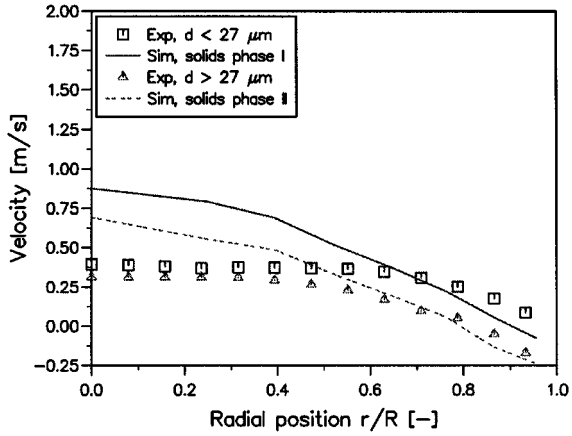

Figure 15. Particle velocity profiles, $V_{sup} = 0.7$ m/s, 0.4 kg solids.

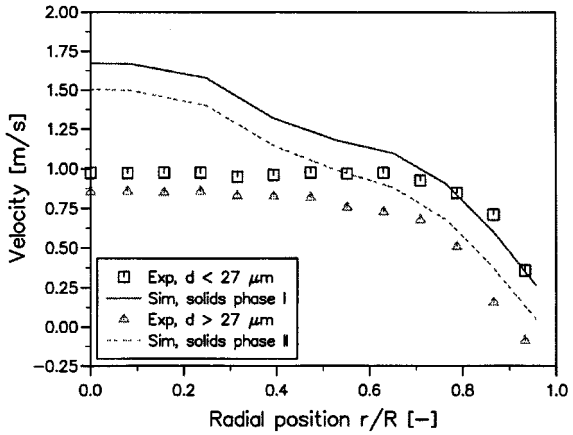

Figure 16. Particle velocity profiles, $V_{sup} = 1.4$ m/s, 0.4 kg solids.

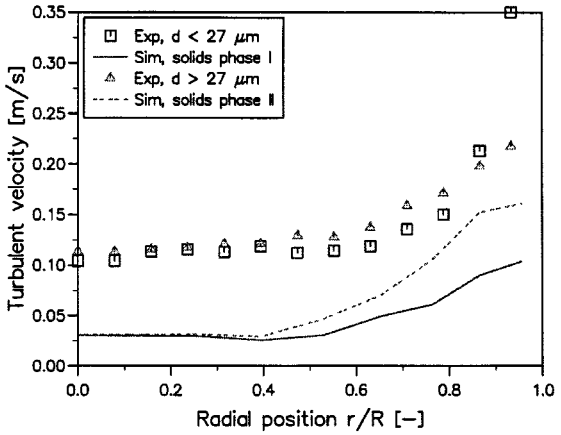

Figure 18. RMS velocity profiles, $V_{sup} = 1.4$ m/s, 0.1 kg of solids.

riser part of the circulating fluidized bed was considered, and the riser was assumed to be two-dimensional. The first assumption will influence the solids concentration in the riser and, more important, the inlet and outlet flow conditions. In the simulations, the inlet was assumed to be a one-dimensional plug flow for the gas phase as well as the solid phases. The actual inlet and outlet conditions are nonuniform and cause nonsymmetric flow behavior in the riser. The LDA measurements were performed from the center line to the wall perpendicular to the plane, as shown in Figure 5, and therefore we were not able to capture any nonuniform flow behavior in this direction. A three-dimensional curvilinear or multiblock approach would be more desirable.

The fact that simulation was performed for only two particle sizes while experiments measured the whole range of particles may be major the reason for the deviations between measurements and simulations.

RMS velocity profiles

Figures 17, 18, 19, and 20 show the experimental particle RMS velocity profiles for each particle group as well as the computed RMS velocities. Since solid concentration was very low, it is expected that the fluctuating velocity or the particle-phase turbulence is caused mainly by the shear and particle collisions with the wall. The RMS velocity for all runs increased from the center of the riser toward the wall. Our experimental results showed that the particle RMS velocity is of the same order of magnitude for all flow conditions. However, in the wall region the fluctuating velocity of particles increased with an increase in superficial gas velocity, due to higher velocity gradients.

Overall, the experimental results showed that the RMS velocity is higher for the particles of largest size in very dilute (such as 1–3%) gas/solids flow systems. Our experimental data did not support the behavior reported in the literature where large particles normally are assumed to have less fluctuating behavior. The gas turbulence is normally less than the solid turbulence. Smaller particles follow the gas flow pattern more easily than larger particles. This may explain why in very dilute gas/solids flow systems with few particle collisions, the fluctuating velocity of the larger particles is higher than the smaller particles.

The computed particle turbulent velocity showed the same form and behavior as the experimental data. Similar to the

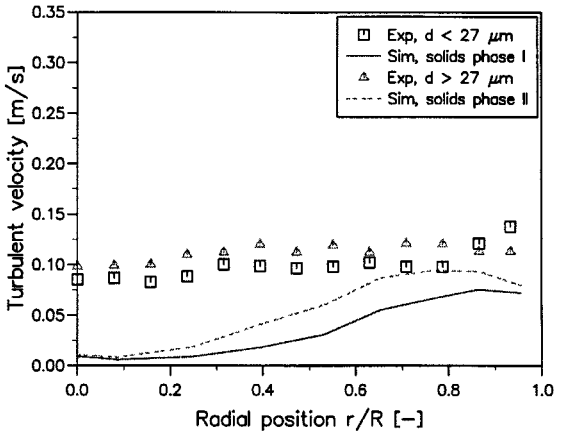

Figure 17. RMS velocity profiles, $V_{sup} = 0.7$ m/s, 0.1 kg solids.

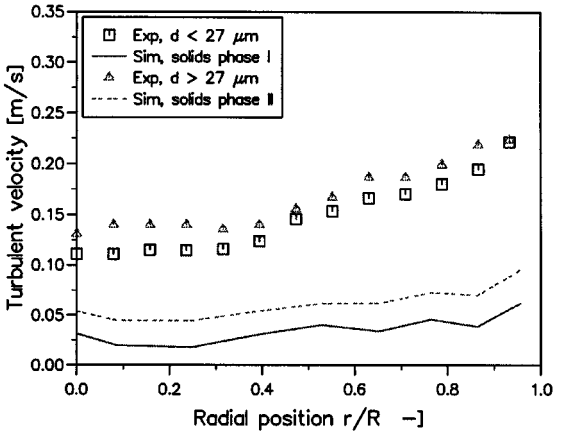

Figure 19. RMS velocity profiles, $V_{sup} = 0.7$ m/s, 0.4 kg solids.

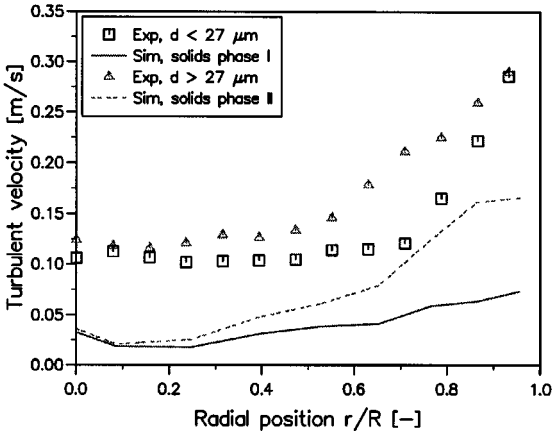

Figure 20. RMS velocity profiles, $V_{sup} = 1.4$ m/s, 0.4 kg solids.

experimental data the computed particle fluctuating velocity showed an increase near the wall. However, RMS velocities are lower than experimental data at all radial locations. In the turbulent kinetic energy equation a dissipation term due to interaction between the gas and solids phases is included, whereas the corresponding production term is neglected. Ding and Gidaspow (1990) argued that this production term could be neglected. Based on our experimental data there may be reasons to believe that this term should be included.

Although we cannot clearly express the extent of accuracy using two granular temperature equations, since our experimental data showed slightly different particles fluctuating for particles of different size, we believe that two equations in general are more capable of describing flow patterns.

Since we did not measure any particle size larger than the largest particle initially in the bed, we assumed the cluster formation is minimized in our very dilute riser.

Conclusions

An experimental study of the flow behavior of group A particles in the riser section of a laboratory-scale circulating fluidized bed using LDA and a modified Shape Discrimination Technique was successfully conducted. Particle diameter and mean and fluctuating velocity for different particle sizes were measured for different flow conditions. The experimental results showed that there was no significant agglomeration in the gas/solids flow system. Typical annulus-core flow behavior was observed and a relative velocity between particles of different sizes was measured. Different fluctuating velocity of different particle sizes was observed. The largest particles showed the highest fluctuating velocity. This behavior was caused by significant gas/solids interactions. A significant radial segregation of the particles of different sizes was also observed. The mean particle diameter increased from the center of the riser toward the wall.

A computational fluid dynamics (CFD) multiphase gas/solids model was presented. The model is based on a Eulerian description of the phases where the kinetic theory for granular flow forms the basis for the turbulence modeling in the solids phases. The model was generalized for one gas phase and N number of solids phases to provide a realistic description of particle-size distributions and a nonuniform diameter distribution in gas/solids systems. Each solid phase was characterized by diameter, form factor, density, and restitution coefficient. The granular temperature and momentum equations were solved for each phase.

A computational study of the riser section of the circulating fluidized bed was performed using two different particle sizes. Although some discrepancies between calculated values and experimental data were observed, the observed core-annulus flow with a correct relative velocity between the solid phases was calculated. The discrepancies between simulations and experimental results can be explained by the differences in actual and simulated geometry and particle-size distribution. The simulations were performed using a two-dimensional Cartesian system, but the actual geometry was three-dimensional. The computed fluctuating velocity showed lower values than the experimental data, but demonstrated the same form and behavior. To accurately predict radial segregation of particles and particle velocity, a larger number of solid phases should be considered.

Acknowledgment

This work was financially supported by Norsk Hydro, Statoil, and the Research Council of Norway (NFR).

Literature Cited

Agarwal, P., and J. Sinclair, ''Flow Behavior in Pneumatic Conveying Systems Involving a Binary Particle Mixture,'' *Fluidization*, Vol. IX, L. S. Fan and T. M. Knowlton, eds., Engineering Foundation, New York, p. 477 (1998).

Ahmadi, G., and M. Shahinpour, ''A Kinetic Model for Rapid Flows of Granular Materials,'' *Int. J. Non-Linear Mech.*, **19**, 177 (1983a).

Ahmadi, G., and M. Shahinpour, ''A Note on Collision Operators in Rapid Granular Flows of Rough Inelastic Particles,'' *Powder Technology*, **35**, 119 (1983b).

Andrews, D. G., and H. S. Seifert, ''Investigation of Particle-Size Determination from the Optical Response of a Laser Doppler Velocitymeter,'' *SUDAAR*, 435 (1971).

Arastoopour, H., and D. Gidaspow, ''Analysis of IGT Pneumatic Conveying Data and Fast Fluidization Using a Thermodynamic Model,'' *J. Powder Technology*, **22**, 77 (1979).

Arastoopour, H., S. C. Lin, and S. A. Weil, ''Analysis of Vertical Pneumatic Conveying of Solids Using Multiphase Flow Models,'' *AIChE J.*, **28**, 467 (1982).

Arastoopour, H., and S. Shao, ''Laser Doppler Anemometry: Application in Multiphase Flow Systems,'' *Non-Invasive Monitoring of Multiphase Flows*, J. Chaouki, F. Larachi, and M. P. Dudukovic, eds., Elsevier, The Netherlands (1997).

Arastoopour, H., and Y. Yang, ''Experimental Studies on Dilute Gas and Cohesive Particles Flow Behavior Using Laser Doppler Anemometer,'' *Fluidization*, Vol. VII, O. E. Potter and D. J. Nicklin, eds., Engineering Foundation, New York (1992).

Azario, E., L. Tadrist, R. Santinini, and J. Pantaloni, ''Velocity Analysis of the Solid Phase in Circulating Fluidized Bed,'' *Proc. 2nd Int. Conf. on Multiphase Flow*, Vol. 4, Kyoto, Japan (1995).

Bachalo, W. D., and M. J. Houser, ''Phase Doppler Spray Analyzer for Simultaneous Measurements of Drop Size and Velocity Distributions,'' *Opt. Eng.*, **25**, 583 (1984).

Bachalo, W. D., and M. J. Houser, ''Experiments in Polydispersed Two-Phase Turbulent Flows,'' *2nd Int. Symp. on Laser Anemometry*, Vol. 33, ASME, FED, New York, p. 35 (1985).

Bagnold, R. A., ''Experiments on a Gravity-Free Dispersion of Large Solid Spheres in a Newtonian Fluid Under Shear,'' *Proc. Roy. Soc.*, **A225**, 49 (1954).

Benyahia, S., H. Arastoopour, and T. M. Knowlton, ''Predictions of Solid and Gas Flow Behavior in a Riser Using a Computational

Multiphase Flow Approach,'' *Fluidization*, Vol. IX, L. S. Fan and T. M. Knowlton, eds., Engineering Foundation, New York (1998).
Berkelmann, K. G., and U. Renz, *Applications of Laser Anemometry to Fluid Mechanics*, R. J. Adrian, T. Asanuma, D. F. G. Durao, F. Durst, and J. H. Whitelaw, eds., Spring-Verlag, Berlin (1989).
Birchenough, A., and J. S. Mason, ''Local Particle Velocity Measurements with a Laser Anemometry in an Upward Flowing Gas-Solid Suspension,'' *Powder Technology*, **14**, 139 (1976).
Burge, S. W., *FORCE2— A Multidimensional Flow Program for Gas Solids Flow*, Vol. I, *User's Guide*, Vol. II, *Theory Guide*, Babcock & Wilcox, Alliance, OH, p. 4911-10-01 (1991).
Chapman, S., and T. G. Cowling, *The Mathematical Theory of Non-Uniform Gases*, 3rd ed., Cambridge Univ. Press, Cambridge (1970).
Chen, C. P., ''A Turbulence Closure Model for a Dilute Gas-Particle Flows,'' *Can. J. Chem. Eng*., **63**, 349 (1985).
Deardorff, J. W., ''On the Magnitude of the Subgrid Scale Eddy Coefficient,'' *J. Comput. Phys*., **7**, 120 (1971).
Ding, J., and D. Gidaspow, ''Bubbling Fluidization Model Using Kinetic Theory of Granular Flow,'' *AIChE J.*, **36**, 523 (1990).
Driscoll, J. F., and D. Mann, ''Submicron Particle Size Measurements in an Acetylene/Oxygen Flame,'' Int. Workshop on Laser Velocimetry, Purdue Univ., West Lafayette, IN (1978).
Dunning, J. W., Jr., ''Application of Laser Homodyne Spectrometer to Particle Size Measurements,'' PhD Thesis, School of Engineering, Case Western Reserve University, Cleveland, OH (1967).
Durst, F., and M. Zare, ''Laser-Doppler Measurements in Two-Phase Flows,'' *Proc. LDA-Symp.*, Copenhagen, p. 403 (1975).
Elghobashi, S. E., and T. W. Abou-Arab, ''A Two-Equation Turbulence Model for Two-Phase Flow,'' *Phys. Fluids*, **26**, 931 (1983).
Ergun, S., ''Fluid Flow Through Packed Columns,'' *Chem. Eng. Prog*., **48**, 89 (1952).
Farmer, W. M., ''Measurement of Particle Size, Number Density and Velocity Using a Laser Interferometer,'' *Appl. Opt*., **11**, 2603 (1972).
Farrell, M., C. K. K. Lun, and S. B. Savage, ''A Simple Kinetic Theory for Granular Flow of Binary Mixtures of Smooth, Inelastic Spherical Particles,'' *Acta Mech*., **63**, 45 (1986).
Geldart, D., ''Types of Gas Fluidization,'' *Powder Technology*, **7**, 285 (1973).
Gidaspow, D., *Multiphase Flow and Fluidization. Continuum and Kinetic Theory Descriptions*, Academic Press, Boston (1994).
Grehan, G., G. Gouesbet, R. Kleine, U. Renz, and J. Wilhelmi, *Proc. 3rd Int. Symp. on Applications of Laser Doppler Anemometry to Fluid Mechanic*, Vol. 20 (1982).
Hardalupas, Y., A. M. K. P. Taylor, and J. H. Whitelaw, ''Depth of Field Considerations in Particle Sizing Using the Phase Doppler Technique,'' *Applications of Laser Anemometry to Fluid Mechanics*, R. J. Adrian, T. Asanuma, D. F. G. Durao, F. Durst, and J. H. Whitelaw, eds., Ladoan Instituto Superior Technico, Lisboa, Portugal (1988).
Hishida, K., M. Maeda, J. Imaru, K. Hironaga, and H. Kato, ''Measurements of Size and Velocity of Particle in Two-Phase Flow by a Three-Beam LDA System,'' *Laser Anemometry in Fluid Mechanics*, R. J. Adrian, D. F. G. Durao, F. Durst, H. Mishina, and J. H. Whitelaw, eds., Ladoan Instituto Superior Technico, Lisboa, Portugal (1984).
Jackson, T. A., and G. S. Samuelsen, ''Droplet Sizing Interferometry: A Comparison of the Visibility Technique and Phase Doppler Technique,'' *Applications of Laser Anemometry to Fluid Mechanics*, R. J. Adrian, T. Asanuma, D. F. G. Durao, F. Durst, and J. H. Whitelaw, eds., Ladoan Instituto Superior Technico, Lisboa, Portugal (1988).
James, R. N., W. R. Babock, and H. S. Seifert, ''A Laser Doppler Technique for the Measurement of Particle Velocity,'' *AIAA J*., **6**, 160 (1968).
Jenkins, J. T., and F. Mancini, ''Balance Laws and Constitutive Relations for Plane Flows of a Dense Binary Mixture of Smooth, Nearly Elastic Circular Disks,'' *J. Appl. Mech*., **54**, 27 (1987).
Jenkins, J. T., and S. B. Savage, ''A Theory for the Rapid Flow of Identical, Smooth, Nearly Elastic, Spherical Particles,'' *J. Fluid Mech*., **30**, 187 (1983).
Kim, H. S., and H. Arastoopour, ''Simulation of FCC Particles Flow Behavior in a CFB Using Modified Kinetic Theory,'' *Can. J. Chem. Eng*., **73**, 603 (1995).
Kuipers, J. A. M., K. J. van Duin, F. P. H. van Beckum, and W. P. M. van Swaaij, ''Computer Simulation of the Hydrodynamics of a Two-Dimensional Gas-Fluidized Bed,'' *Comput. Chem. Eng*., **17**, 839 (1993).
Kunii, D., and O. Levenspiel, *Fluidization Engineering*, 2nd ed., Butterworth-Heinemann, Boston (1991).
Lazaro, B. J., ''Evaluation of Phase Doppler Particle Sizing in the Measurement of Optically Thick, High Number Density Sprays,'' United Technologies Research Center, East Hartford, CT (1991).
Lee, S. L., and J. Srinivasan, ''Measurements of Local Size and Velocity Probability Density Distribution in Two-Phase Suspension Flows by Laser Doppler Techniques,'' *Int. J. Multiphase Flow*, **4**, 141 (1978).
Lesinski, J., B. Mizera-Lesinska, J. C. Fanton, and M. I. Boulos, ''Laser Doppler Anemometry Measurements in Gas-Solid Flow,'' *AIChE J.*, **27**, 358 (1981).
Lun, C. K. K., and S. B. Savage, ''A Simple Kinetic Theory for Granular Flow of Rough, Inelastic Spherical Particles,'' *J. Appl. Mech*., **57**, 47 (1987).
Lun, C. K. K., S. B. Savage, D. J. Jeffrey, and N. Chepurniy, ''Kinetic Theories for Granular Flow: Inelastic Particles in Couette Flow and Slightly Inelastic Particles in a General Flowfield,'' *J. Fluid Mech*., **140**, 223 (1984).
Lyczkowski, R. W., and J. X. Bouillard, *Interim User's Manual for FLUFIX/MOD1: A Computer Program for Fluid-Solids Hydrodynamics*, Argonne National Laboratory, Argonne, IL (1989).
Ma, D., and G. Ahmadi, ''A Thermodynamical Formulation for Dispersed Multiphase Turbulent Flows I,'' *Int. J. Multiphase Flows*, **16**, 323 (1990a).
Ma, D., and G. Ahmadi, ''A Thermodynamical Formulation for Dispersed Multiphase Turbulent Flows II,'' *Int. J. Multiphase Flows*, **16**, 341 (1990b).
Manger, E., ''Modelling and Simulation of Gas/Solids Flow in Curvilinear Coordinates,'' PhD Thesis, Telemark College, Porsgrunn, Norway (1996).
Mathiesen, V., ''An Experimental and Computational Study of Multiphase Flow Behavior in Circulating Fluidized Beds,'' PhD Thesis, Telemark College, Porsgrunn, Norway (1997).
Mathiesen, V., T. Solberg, E. Manger, and B. H. Hjertager, ''Modelling and Predictions of Multiphase Flow in a Pilotscale Circulating Fluidized Bed,'' *Circulating Fluidized Bed Technology*, Vol. V, J. Kwauk and J. Li, eds., Science Press, Beijing, China (1997).
Mathiesen, V., T. Solberg, and Hjertager, ''A Computational Study of Multiphase Flow Behavior in a Circulating Fluidized Bed with Realistic Particle Size Distribution,'' *Proc. 3rd Int. Conf. on Multiphase Flow*, Lyon, France (1998).
Mathiesen, V., T. Solberg, and B. H. Hjertager, ''An Experimental and Computational Study of Multiphase Flow Behavior in a Circulating Fluidized Bed,'' *Int. J. Multiphase Flow* (1999).
Rowe, P. N., ''Drag Forces in a Hydraulic Model of a Fluidized Bed: II,'' *Trans. Inst. Chem*., **39**, 175 (1961).
Saffmann, M., P. Buchhave, and H. Tanger, ''Simultaneous Measurements of Size Concentration and Velocity of Spherical Particles by a Laser Doppler Method,'' *Laser Anemometry in Fluid Mechanics*, Vol. II, R. J. Adrian, D. F. G. Durano, F. Durst, H. Mishina, and J. H. Whitelaw, eds., Ladoan Instituto Superior Technico, Lisboa, Portugal (1984).
Samuelsberg, A., and B. H. Hjertager, ''An Experimental and Numerical Study of Flow Patterns in a Circulating Fluidized Bed Reactor,'' *Int. J. Multiphase Flow*, **22**, 575 (1996a).
Samuelsberg, A., and B. H. Hjertager, ''Computational Modelling of Gas Particle Flow in a Riser,'' *AIChE J.*, **42**, 1536 (1996b).
Shao, S., and H. Arastoopour, ''The Flight Time Technique for Simultaneous Measurements of Particle Flow Parameters Using a Laser Doppler Anemometer (LDA),'' *Proc. Fluidization VIII*, Tours, France (1995).
Sinclair, J. L., and R. Jackson, ''Gas-Particle Flow in a Vertical Pipe with Particle-Particle Interactions,'' *AIChE J.*, **35**, 1473 (1989).
Syamlal, M., W. Rogers, and T. J. O'Brien, *MFIX Documentation Theory Guide*, Tech. Note DOE/METC-94/1004, U.S. Dept. of Energy, Morgantown Energy Technology Center, Morgantown, WV (1993).
Tadrist, L., E. Azario, and P. Cattieuw, ''Analysis of Two-Phase Flow in a Circulating Fluidized Bed,'' *Proc. Int. Conf. on Circulating Fluidized Bed*, p. 702 (1993).

Tsuji, Y., Y. Morikawa, and H. Shiomi, ''LDV Measurements of an Air-Solid Two-Phase Flow in a Vertical Pipe,'' *J. Fluid Mech*., **130**, 417 (1984).
Tsuo, Y. P., and W. Gidaspow, ''Computation of Flow Patterns in Circulating Fluidized Beds,'' *AIChE J.*, **36**, 885 (1990).
Van Den Moortel, T., R. Santini, and L. Tadrist, ''Measurement of Local Mass Flux in a Circulating Fluidized Bed Using a Phase Doppler Particle Analyzer: A New Post-Processing Data Algorithm,'' *Proc. ASME Heat Transfer Division*, **3**, 239 (1996).
Wen, C. Y., and Y. H. Yu, ''Mechanics of Fluidization,'' *Chem. Eng. Prog. Symp. Series*, **62**, 100 (1966).
Yakhot, Y., and S. A. Orszag, ''Renormalization Group Analysis of Turbulence. 1. Basic Theory,'' *J. Sci. Comput*., **1**, 3 (1986).
Yang, Y., ''Experiments and Theory on Gas and Cohesive Particles Flow Behavior and Agglomeration in the Fluidized Bed Systems,'' PhD Thesis, Illinois Institute of Technology, Chicago (1991).
Zhang, Y. F., and H. Arastoopour, ''Dilute FCC Particles/Gas Flow Behavior in the Riser of a Circulating Fluidized Bed,'' *Powder Technology*, **84**, 221 (1995).
Zhang, Y. F., Y. Yang, and H. Arastoopour, ''Electrostatic Effect on the Flow Behavior of a Dilute Gas/Cohesive Particle Flow System,'' *AIChE J.*, **42**, 1590 (1996).

Manuscript received Dec. 11, 1998, and revision received June 1, 1999.